

TARGET RECOGNITION FOR MULTI-ASPECT SAR IMAGES WITH FUSION STRATEGIES

Ruohong Huan^{1, *} and Yun Pan²

¹College of Computer Science and Technology, Zhejiang University of Technology, Hangzhou, China

²Department of Information Science and Electronic Engineering, Zhejiang University, Hangzhou, China

Abstract—Two fusion strategies for target recognition using multi-aspect synthetic aperture radar (SAR) images are presented for recognizing ground vehicles in MSTAR database. Due to radar cross-section variability, the ability to discriminate between targets varies greatly with target aspect. Multi-aspect images of a given target are used to support recognition. In this paper, two fusion strategies for target recognition using multi-aspect SAR images are proposed, which are data fusion strategy and decision fusion strategy. The recognition performance sensitivity to the number of images and the aspect separations is analyzed for those two target recognition strategies. The two strategies are also compared with each other in probability of correct classification and operating efficiency. The experimental results indicate that if we have a small number of multi-aspect images of a target and the aspect separations between those images are proper, the probability of correct classification obtained by the two proposed strategies can be advanced significantly compared with that obtained by the method using single image.

1. INTRODUCTION

Synthetic aperture radar (SAR) image target recognition is a key issue in SAR image interpretation and analysis. Before target recognition, detecting targets in images is generally required [1]. When a target is detected and its position is known in the SAR image, target recognition is then implemented to achieve its class and type [2, 3]. Preprocessing, feature extraction, and classification are three essential steps in

Received 3 October 2012, Accepted 7 November 2012, Scheduled 25 November 2012

* Corresponding author: Ruohong Huan (huanrh@zjut.edu.cn).

target recognition [4, 5]. Feature extraction and classification are the most important two steps which mainly determine the recognition performance of a target recognition method.

SAR images are highly sensitive to target aspect, due to shadowing effects, interaction of the signature with the environment, projection of a three dimensional scene onto a slant plane and other reasons due to the aspect dependence of radar cross-sections [6, 7]. The ability to discriminate between targets in SAR images also varies greatly with target aspect. Multiple images of a target in different aspects, i.e., multi-aspect images, may provide more robust classification performance than single image. Thus, we take two questions into account, which are how many multi-aspect images are required to achieve significant improvement and what is the aspect separation between them.

Brendel and Horowitz [8] presented an analysis of the fundamental benefits of aspect diversity for SAR automatic target recognition (ATR). Multi-aspect diversity was incorporated into an existing SAR ATR classifier, which was a mean squared error (MSE)-template-based ATR system. Then, multi-aspect processing can be implemented by summing the MSE scores of the individual aspect images of the same target to form the result of having one grand multi-aspect reference image. Multiple views separated by 60 degree up to 4 aspects for a total of 180 degree from the first view were used in their experiments. And performance enhancement by the aspect diversity for SAR ATR was illustrated in the results. Bhanu and Jones [9] used the fundamental azimuthal variance of SAR scatterer locations as the basis for a principled approach to multiple look angle SAR recognition. The experimental results in the paper demonstrated that SAR recognition results at different azimuths are independent. In addition, they show that decision level fusion of two observations at different look angles can substantially increase SAR recognition performance. Ettinger and Snyder [10, 11] developed model-based approaches to SAR ATR by fusing multiple images of same vehicle collected at different angles. Two high-level multi-aspect fusion approaches, namely decision-level and hypothesis-level fusion were evaluated quantitatively. They demonstrated that fusing multiple looks gives significant improvements in probability of identification even with only two or three SAR looks differing by small angles. Brown [7] developed a Bayesian approach to multi-aspect target classification and considered the aspect dependence of ATR performance. The author addressed four specific questions about multi-aspect target recognition, and discussed the classification performance benefits by employing at most three incoherent images of a target and with the angular separation of 5 degree, 15 degree, 45

degree and 60 degree. Vespe et al. [12] developed a multi-perspective target classification method, which used Function Neural Networks (RBFNNs) to combine multiple views of a target collected by different locations. Two-perspective benefits have been illustrated in terms of correct classification rates given by aspect diversification.

In the above literatures, various approaches have been proposed for SAR target recognition using multi-aspect images and testified the benefits in recognition performance by using multi-aspect images over single image. However, the answers to the two questions about multi-aspect target recognition were not comprehensive. Most of the research just took two or three multi-aspect images into account. Almost none of them discussed the effect of aspect separation of images on the recognition performance, except literature [7] analyzed the classification performance in four different angular separations, which are 5 degree, 15 degree, 45 degree and 60 degree. In this paper, two fusion strategies for target recognition using multi-aspect SAR images are proposed, which are data fusion strategy and decision fusion strategy. At most six views and every angular separation ranging from 1 degree to 360 degree are considered for performance evaluation. Ten types of ground vehicles in the Moving and Stationary Target Acquisition and Recognition (MSTAR) public release database are taken for experiments. The recognition performance sensitivity to the number of images and the aspect separation of those two target recognition strategies is analyzed. The two strategies are compared with each other in probability of correct classification and operating efficiency. Also, the probabilities of correct classification obtained by the two strategies are compared with that obtained by the method using single SAR image.

This paper is organized as follows: experimental data is presented in Section 2. Target recognition method for SAR single image is described in Section 3. Section 4 covers data fusion strategy and decision fusion strategy. Experimental results and analysis are presented in Sections 5. Section 6 concludes the paper and discusses the future research directions.

2. DATA PREPARATION

In this paper, SAR chips included in DARPA MSTAR Program database are used. The publicly released portion of the MSTAR database contains SAR images of ten military vehicles, including BMP2 (tank), BTR70 (armored car), T72 (tank), BTR_60 (armored car), 2S1 (cannon), BRDM.2 (truck), D7 (bulldozer), T62 (tank), ZIL_131 (truck), and ZSU_23/4 (cannon). All of those vehicles are

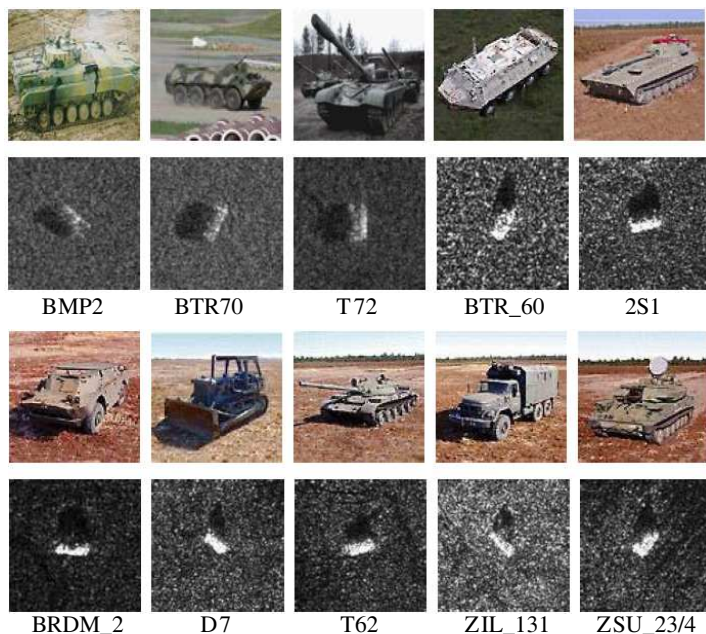


Figure 1. Optical images and SAR images for ten class targets.

used in our experiments. Each of the targets has views at 15° and 17° depression angles. The data in depression 17° are used for training and the other for testing. There are about 190–300 different aspect versions of each target at each depression angle. Table 1 lists the type and sample number of training and testing set. Figure 1 depicts optical images and SAR images for those ten class targets. Figure 2 depicts multiple images of a target in the same depression angle but in different aspects.

3. TARGET RECOGNITION FOR SAR SINGLE IMAGE

SAR target recognition method for single image presented in this paper consists of three steps as shown in Figure 3, which are preprocessing, feature extraction, and classification. The specific approaches or algorithms used for each step are described respectively below.

3.1. Preprocessing

Some feature extraction algorithms and classification algorithms are sensitive to location shift, rotation, and non-uniform illumination [4].

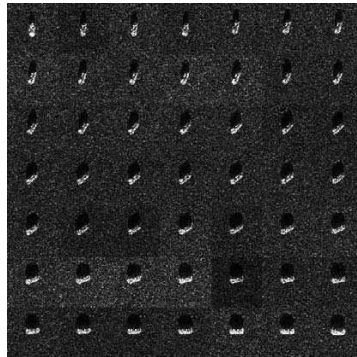


Figure 2. Multiple images of a target in the same depression angle but in different aspects.

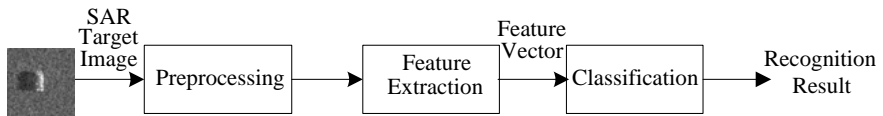


Figure 3. Diagram of SAR target recognition for single image.

Table 1. Type and sample number of training and testing set.

Training Set	Sample Number	Testing Set	Sample Number
BMP2_c21	233	BMP2_c21	196
BTR70_c71	233	BMP2_9563	195
T72_132	232	BMP2_9566	196
BTR_60	256	BTR70_c71	196
2S1	299	T72_132	196
BRDM_2	298	T72_812	195
D7	299	T72_s7	191
T62	299	BTR_60	195
ZIL_131	299	2S1	274
ZSU_23/4	299	BRDM_2	274
		D7	274
		T62	273
		ZIL_131	274
		ZSU_23/4	274

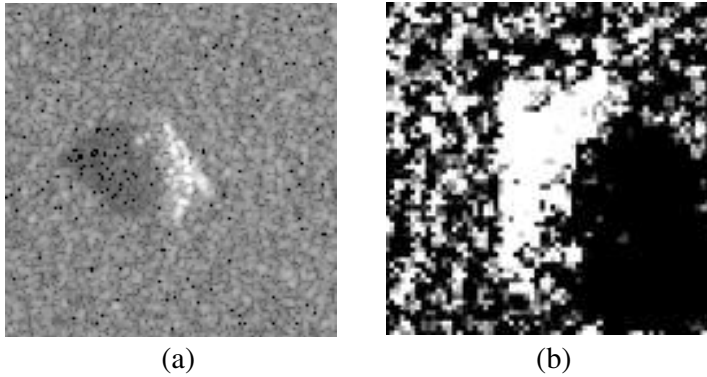


Figure 4. (a) and (b) depict the chip of target T72 before and after preprocessing.

Thus, preprocessing is necessary. In this paper, we first rotate each target to a vertical orientation using ground truth information to bring the targets into a standardized target orientation. Then, highest energy reflecting point of the target chip is found and located to the centre of a new chip, the size of which is 64 pixels by 64 pixels. The final preprocessing step is to normalize the target chips. Normalization alters the pixel values such that, the mean intensity is zero and the standard deviation value is one for each chip. Figures 4(a) and (b) respectively depict the chip of target T72 before and after preprocessing.

3.2. Feature Extraction Using Wavelet Domain PCA

Feature extraction is an important step in the target recognition process. Feature extraction algorithms extract unique target information or signature from each chip [13–17]. 2-D wavelet transformation is used here to perform 3 levels decomposition to each chip. The sketch map of 3 levels 2-D wavelet transformation is shown in Figure 5(a), where LL_i denotes low frequency component from the outcomes of the i levels decomposition; LH_i , HL_i , and HH_i denote high frequency sub images which contain specific information from the outcomes of the i levels decomposition. Figure 5(b)-2 is the decomposition results of Figure 5(b)-1 by 3 levels 2-D wavelet decomposition.

LL_3 , which contains low frequency component from the outcomes of 3 levels decomposition of each chip is picked for the following operation. We first transform LL_3 to a 64-D column vector, as the

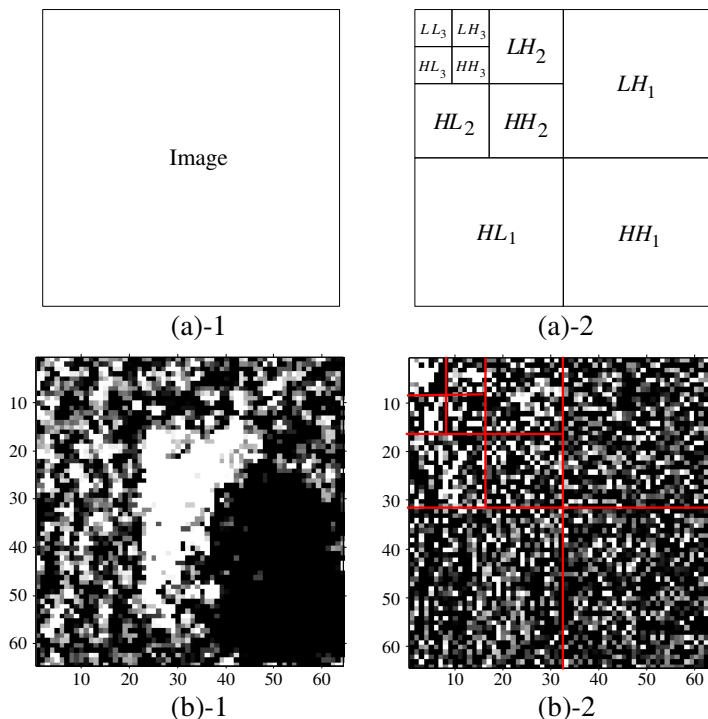


Figure 5. (a) Sketch map of 3 levels 2-D wavelet transformation, (b) decomposition results of target T72.

size of it is 8 pixels by 8 pixels originally. Then, principal component analysis (PCA) is applied for feature extraction. Extract column vectors transformed from LL_3 from all the training chips to form a data matrix $\mathbf{X}_{m \times n}$, where $m = 64$ and n is the sample number of the training set. Then, the correlation matrix $\mathbf{C} = E[\mathbf{X}_{m \times n} \mathbf{X}_{m \times n}^T]$ is calculated. By solving the eigenvalue equation $\lambda \xi = \mathbf{C} \xi$, the eigenvectors ξ_i and eigenvalues λ_i , $i = 1, 2, \dots, m$, are obtained. The eigenvectors ξ_i with the largest p eigenvalues λ_i are selected as the orthonormal vector basis of the chip database. p is supposed to be 30 here, as the probability of correct classification could attain the highest when $p = 30$ in our experiments. The transformation matrix \mathbf{W} is formed from those p eigenvectors in the column manner, that is $\mathbf{W} = [\xi_1 \xi_2 \dots \xi_p]^T$. Given an input data \mathbf{x} , which is a certain 64-D column vector transformed from LL_3 , p -D feature vectors \mathbf{y} of the input data \mathbf{x} can be acquired by computing the equation $\mathbf{y} = \mathbf{W} \cdot \mathbf{x}$. Through this process, we get a 30-D feature vector for each chip. Figure 6 shows

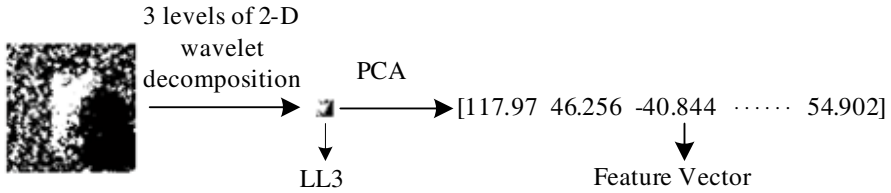


Figure 6. Process of feature extraction.

the process of feature extraction, where left is the preprocessed image, middle is LL_3 after 3 levels 2-D wavelet decomposition and right is feature vectors obtained by PCA algorithm.

3.3. Classification Using Support Vector Machine (SVM)

Using the extracted feature vectors, the classifier must be able to correctly decide which class the target belongs to. In this paper, SVM is used as classifier. SVM, as a method of learning and separating binary classes, is superior in classification performance, and has been in the spotlight for SAR classification or recognition [13, 18–20]. The basic principle of SVM can be generalized as follows [19, 21]: mapping the data to a high-dimensional Euclidean space (feature space) using a nonlinear mapping $\phi: R^n \rightarrow E$, finding the decision surface in the new feature space, using kernel function for nonlinear mapping. Therefore, an arbitrary feature vector \mathbf{x} can be classified by

$$f(x) = \text{sgn} \left\{ \sum_{i=1}^l \alpha_i^* y_i K(\mathbf{x}_i, \mathbf{x}) + b^* \right\} \quad (1)$$

where \mathbf{x}_i is support vector, $y_i \in \{-1, 1\}$ is class label corresponded to \mathbf{x}_i , $K(\mathbf{x}_i, \mathbf{x})$ is kernel function, α_i^* is Lagrange multiplier corresponded to \mathbf{x}_i , b^* is classification threshold value and sgn is the symbol function.

SVM is a binary classifier in basic. Since our goal is to identify ten types of targets in MSTAR dataset, we need to extend it to multi-class classifier. We first decompose the multi-class problem into several binary problems with one-against-one scheme, and use voting rule for decision making [22]. Gaussian kernel function $K(\mathbf{x}_i, \mathbf{x}) = \exp\{-\frac{|\mathbf{x}-\mathbf{x}_i|^2}{\sigma^2}\}$ is applied as the kernel function for SVM.

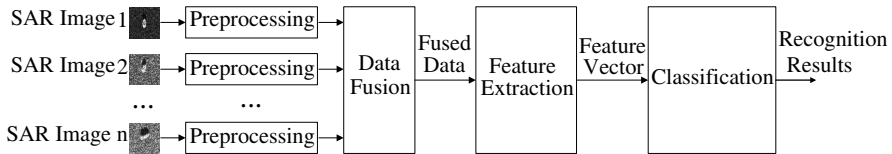


Figure 7. Process diagram of data fusion strategy.

4. TWO FUSION STRATEGIES FOR MULTI-ASPECT SAR IMAGES TARGET RECOGNITION

4.1. Data Fusion Strategy

In data fusion strategy, multiple images of a target in the same depression angle but in different aspects are selected. Each image conducts preprocessing independently. PCA is used to fuse the preprocessed image data. Wavelet domain PCA is employed to extract feature vectors from the fused image data. SVM is applied to classify the extracted feature vectors to obtain recognition results. The process diagram of data fusion strategy is shown in Figure 7, where the implemental methods of preprocessing, feature extraction and classification are identical with those in target recognition for SAR single image.

4.2. Decision Fusion Strategy

In decision fusion strategy, multiple images of a target in the same depression angle but in different aspects are selected, which is the same as the first step in data fusion strategy. Each image conducts preprocessing, feature extraction and classification independently. Ranking based decision fusion approach is used to fuse the outputs of the classifiers. The final recognition results are attained from the output of the fuser [23, 24]. The process diagram of decision fusion strategy is shown in Figure 8. The specific methods of preprocessing, feature extraction and classification are the same as those in target recognition for SAR single image.

4.3. Fusion Algorithms Used in Two Strategies

4.3.1. PCA Based Data Fusion Algorithm

PCA is a well-known statistical method that has been used for data fusion. As it was proved to be a better fusion tool over some other fusion algorithms (like DWT) [25], we use it here.

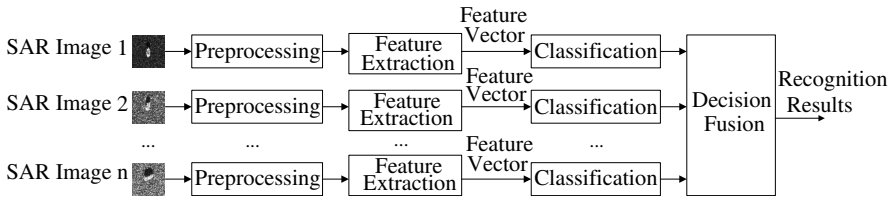


Figure 8. Process diagram of decision fusion strategy.

Supposing $\mathbf{x}_1, \mathbf{x}_2, \mathbf{x}_3, \dots, \mathbf{x}_N$ denote original image data, and those data are all arranged by rows (supposing each image has M pixels). N is the total number of images used in the fusion. Each original image \mathbf{x}_j is inserted into a 2-D matrix \mathbf{X} as its j th row. Finally, a N -by- M 2-D matrix \mathbf{X} is achieved. Calculate the covariance matrix \mathbf{C} of \mathbf{X} . Eigenvectors of the covariance matrix can be obtained by solving the eigenvalue equation

$$\lambda \xi = \mathbf{C} \xi \quad (2)$$

Normalize the eigenvector ξ_1 corresponding to the largest eigenvalue λ_1 as

$$\bar{\xi}_{1j} = \frac{\xi_{1j}}{\sum_{j=1}^N \xi_{1j}} \quad (3)$$

where ξ_{1j} is the j th component in ξ_1 . The fused image data \mathbf{y} can be represented by

$$\mathbf{y} = \sum_{j=1}^N \bar{\xi}_{1j} \cdot \mathbf{x}_j \quad (4)$$

4.3.2. Ranking Based Decision Fusion Algorithm

Ranking based decision fusion algorithm is one of the typical decision fusion algorithms, used for target recognition. Due to its superior performance over other decision fusion algorithms for target recognition [26,27], we apply it in our experiments. Ranking based decision fusion algorithm can be described as follows.

Suppose that we have a set of K classifiers C_k , each of which classifies targets into one of Q distinct classes, where $k = 1, 2, \dots, K$. The output vector of classifier C_k , given a target \mathbf{x} , is represented by a column vector:

$$\mathbf{y}_k = \{y_{k,q}; q = 1, 2, \dots, Q\} \quad (5)$$

where the q th component of the output vector \mathbf{y}_k represents the estimated posterior probability that target \mathbf{x} belongs to the class q , estimated by classifier C_k . $y_{k,q}$ satisfies the following two requirements:

$$0 \leq y_{k,q} \leq 1 \tag{6}$$

$$\sum_{q=1,2,\dots,Q} y_{k,q} = 1 \tag{7}$$

The classification decision of classifier C_k is:

$$\theta_k = \arg \max_{1 \leq q \leq Q} y_{k,q} \tag{8}$$

In ranking based decision fusion technique [26, 27], a new vector \mathbf{z}_k is generated for the classifier C_k . In \mathbf{z}_k , each component is assigned a score that is based on the rank of that component in the output vector $\mathbf{y}_k = \{y_{k,q}; q = 1, 2, \dots, Q\}$. That is, $\mathbf{z}_k = R(\mathbf{y}_k)$, where R is a ranking operator that takes in a vector $\mathbf{y}_k = \{y_{k,q}; q = 1, 2, \dots, Q\}$ and substitutes it for a new vector $\mathbf{z}_k = \{z_{k,q}; q = 1, 2, \dots, Q\}$, where the vector components $z_{k,q}$ are computed as follows:

- Define a ranking vector: $\mathbf{r} = \{r_q; q = 1, 2, \dots, Q\}$.
- Set $r_q = 0$ for all q .
- For $i = 1$ step 1 until Q .

Begin

$$r_i = \arg \max_{1 \leq q \leq Q \text{ and } q \neq r_i \text{ for all } i} y_{k,q} \tag{9}$$

$$z_{k,r_i} = Q - (i - 1) \tag{10}$$

End

This process is repeated for all the contributing components. A final decision θ is then made by employing a Bayesian decision:

$$z_q = \frac{1}{K} \sum_{k=1}^K z_{k,q} \tag{11}$$

$$\theta = \arg \max_{1 \leq q \leq Q} z_q \tag{12}$$

5. EXPERIMENTAL RESULTS AND ANALYSIS

SAR signatures vary greatly with aspect, as shown previously in Figure 2. Thus recognition performance may also be expected to vary with target aspect. Given that this is the case, exploitation of multi-aspect images of a target should provide more robust recognition performance than only using single image. The number of images used

and the aspect separation between them are two issues that affect the final recognition performance of a target.

Our experiments are to examine the recognition performance sensitivity of the two proposed strategies to the number of images and the aspect separations. Probability of correct classification (PCC) is calculated via correct classification sample number dividing by total sample number, which is the most important measurement for recognition performance.

The SAR chips of some aspects in the MSTAR database are absent, so the aspect separations between neighbour chips are not 1 degree for all. For the chip absence, we use the chip closest in aspect to substitute for the needed chip. Thus, the PCC lines received in results may not be thoroughly precise; however, the trend of them has certain reference value.

5.1. Results and Analysis of Data Fusion Strategy

Figure 9 shows PCC lines in data fusion strategy using different number of multi-aspect images with the aspect separation ranging from 1 degree to 360 degree. From Figure 9, we find PCC lines are nearly symmetrical over the aspect separation of 180 degree, when two or three images are data fused. When two images are fused, if the aspect separation is near 0 degree or 180 degree or 360 degree, the PCC obtained is relatively higher. If the aspect separation is close to 90 degree or 270 degree, the PCC obtained is relatively lower. When three images are used for data fusion, if the aspect separation is near 0 degree or 180 degree, the PCC obtained is relatively higher. If the aspect separation is close to 60 degree or 120 degree or 240 degree or

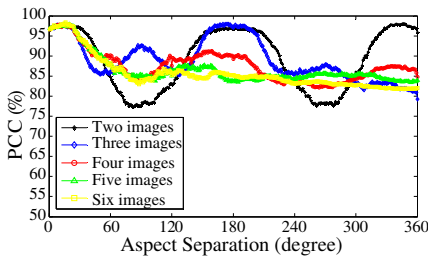


Figure 9. PCCs in data fusion strategy using multi-aspect images with the aspect separation ranging from 1 degree to 360 degree.

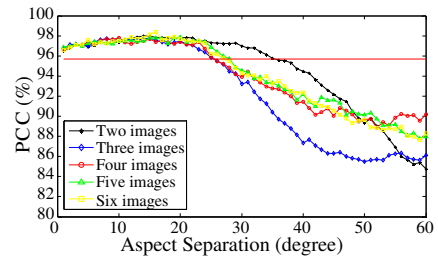


Figure 10. PCCs in data fusion strategy using multi-aspect images with the aspect separation ranging from 1 degree to 60 degree.

300 degree, the PCC obtained is relatively lower. When more than three images are fused, PCC lines tend to decrease with the increasing aspect separation.

Interval of aspect separation between 1 degree and 60 degree is picked out for further observation, which is shown in Figure 10. From Figure 10, we find the PCC lines keep probably stable in a certain aspect separation interval, which may be smaller than 20 degree approximately. In that interval, PCC lines belonged to different number of images are almost similar, which means PCC in that interval has no obvious relationship with the number of used images. Out of that aspect separation interval, the PCC lines tend to decline with the increasing aspect separation. When the aspect separations are less than certain values (thresholds), PCCs are higher than 95.69%, which is the PCC of single image without data fusion drawn as the red line in Figure 10. The thresholds vary with the number of fused images. Table 2 lists the thresholds when two, three, four, five or six multi-aspect images are data fused. In Table 2, we observe the thresholds are all relatively small aspect separations. If more than two images are fused, the thresholds are almost the same.

Table 3 lists the highest PCCs of ten class targets obtained using different number of images in some certain aspect separations (AS) by data fusion strategy. From Table 3, we find the highest PCCs have little relationship with the number of fused images, but they are all in small aspect separations.

By observing Figures 9 and 10, Tables 2 and 3, we can conclude that if relatively small aspect separation is used in multi-aspect images data fusion strategy, higher PCC could be obtained than that gained from single image, and the PCC is not relevant to the number of fused images, when relatively small number images are used. On the other, if too large aspect separation is used in this strategy, PCC may be decreased compared with that obtained from the single image method.

Table 2. Thresholds in data fusion strategy.

	Threshold (degree)
Two images	35
Three images	25
Four images	25
Five images	28
Six images	27

Table 3. Highest PCCs obtained in data fusion strategy (%).

	Single image	Two images (AS is 15°)	Three images (AS is 15°)
BMP2	92.67	94.04	92.16
BTR70	99.49	99.49	99.49
T72	86.43	96.22	97.08
BTR_60	98.46	98.97	100.00
2S1	99.64	99.64	98.91
BRDM_2	98.54	99.64	98.91
D7	98.91	99.64	99.27
T62	98.53	100.00	100.00
ZIL_131	100.00	100.00	100.00
ZSU_23/4	100.00	99.64	100.00
Average	95.69	98.00	97.75
	Four images (AS is 10°)	Five images (AS is 20°)	Six images (AS is 16°)
BMP2	93.02	92.50	94.21
BTR70	100.00	98.47	99.49
T72	96.22	99.14	98.63
BTR_60	100.00	98.97	99.49
2S1	100.00	97.45	99.27
BRDM_2	98.54	98.18	98.18
D7	99.27	99.64	99.64
T62	100.00	99.63	100.00
ZIL_131	100.00	100.00	100.00
ZSU_23/4	99.64	100.00	100.00
Average	97.81	97.88	98.38

5.2. Results and Analysis of Decision Fusion Strategy

Figure 11 shows PCC lines in decision fusion strategy with the aspect separation ranging from 1 degree to 360 degree using different number of multi-aspect images. From Figure 11, we find that when two images are used, PCC is almost constant with the change of aspect separation.

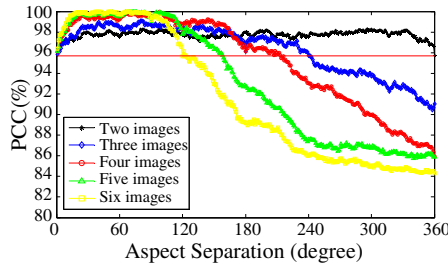


Figure 11. PCCs in decision fusion strategy using multi-aspect images with the aspect separation ranging from 1 degree to 360 degree.

Table 4. Thresholds in decision fusion strategy.

	Threshold (degree)
Two images	None
Three images	241
Four images	213
Five images	158
Six images	121

When more than two images are used, PCCs are nearly constant in certain aspect separation intervals. The more the images used for decision fusion, the smaller the intervals are. Out of those intervals, PCCs decrease acutely with the increasing aspect separation. When the aspect separations are less than certain values (thresholds), PCCs are higher than 95.69%, which is the PCC of single image drawn as the red line in Figure 11. The thresholds vary with the number of fused images. Table 4 lists the thresholds when different numbers of multi-aspect images are decision fused. In Table 4, we observe the thresholds are all relatively large aspect separations (except for two images), and the thresholds decrease with the increasing number of images. When two images are used for decision fusion, PCCs obtained are all higher than the PCC of single image, which means there is no threshold when two images are used.

Table 5 lists the highest PCCs with different number of multi-aspect images in some certain aspect separations (AS) by decision fusion strategy. From Table 5, we find that more images lead to higher PCCs, and when five or more images are used, the PCCs reach 100% in some aspect separations.

From the results in Figure 11, Tables 4 and 5, we conclude that when a small number of images are used, multi-aspect images yield

Table 5. Highest PCCs obtained in decision fusion strategy (%).

	Single view	Two images (AS is 98°)	Three images (AS is 80°)
BMP2	92.67	98.30	99.32
BTR70	99.49	100.00	100.00
T72	86.43	94.33	96.56
BTR_60	98.46	100.00	100.00
2S1	99.64	99.64	100.00
BRDM_2	98.54	98.18	100.00
D7	98.91	98.54	98.18
T62	98.53	100.00	100.00
ZIL_131	100.00	100.00	100.00
ZSU_23/4	100.00	100.00	100.00
Average	95.69	98.35	99.09
	Four images (AS is 98°)	Five images (AS is 71°)	Six images (AS is 39°)
BMP2	100.00	100.00	100.00
BTR70	100.00	100.00	100.00
T72	100.00	100.00	100.00
BTR_60	100.00	100.00	100.00
2S1	100.00	100.00	100.00
BRDM_2	100.00	100.00	100.00
D7	99.64	100.00	100.00
T62	100.00	100.00	100.00
ZIL_131	100.00	100.00	100.00
ZSU_23/4	100.00	100.00	100.00
Average	99.97	100.00	100.00

better recognition results than single image in a relatively wide aspect separation interval. The intervals vary with the change of the number of the used images. And in those intervals, more images result in higher PCCs.

5.3. Comparison of Two Strategies

We take some certain aspect separation intervals to do average of PCCs of the two fusion strategies respectively. The aspect separation intervals range from 5 degree to 60 degree. The average results of the two strategies are shown in Table 6, where DaFu means data fusion

Table 6. Average PCCs in some aspect separation intervals of two fusion strategies.

Interval (degree) /Method	Two images	Three images	Four images	Five images	Six images
5/DaFu	96.90	97.01	97.03	97.05	97.06
5/DeFu	96.68	96.28	96.93	97.03	97.41
10/DaFu	97.10	97.30	97.30	97.21	97.21
10/DeFu	96.93	96.65	97.44	97.63	98.05
15/DaFu	97.35	97.41	97.34	97.33	97.41
15/DeFu	97.06	96.92	97.85	98.11	98.51
20/DaFu	97.47	97.41	97.35	97.42	97.53
20/DeFu	97.14	97.10	98.18	98.48	98.85
25/DaFu	97.49	97.26	97.26	97.40	97.46
25/DeFu	97.24	97.34	98.44	98.74	99.05
30/DaFu	97.44	96.80	96.83	97.09	97.10
30/DeFu	97.36	97.53	98.60	98.89	99.18
35/DaFu	97.29	96.09	96.35	96.61	96.63
35/DeFu	97.42	97.67	98.72	99.01	99.27
40/DaFu	97.02	95.16	95.80	96.08	96.14
40/DeFu	97.46	97.79	98.80	99.11	99.36
45/DaFu	96.59	94.24	95.21	95.58	95.58
45/DeFu	97.49	97.89	98.87	99.17	99.41
50/DaFu	95.99	93.40	94.70	95.06	94.99
50/DeFu	97.54	97.98	98.93	99.23	99.46
55/DaFu	95.30	92.72	94.22	94.56	94.43
55/DeFu	97.58	98.06	98.98	99.29	99.51
60/DaFu	94.47	92.15	93.87	94.02	93.91
60/DeFu	97.59	98.10	99.00	99.31	99.53

Table 7. Running times for recognition of the two fusion strategies under different number of images after preprocessing.

Method	Computational Procedure	Time (ms)
DaFu/2 images	DaFu (2 images) + FE + Cl	$5.2 + 5.9 + 1.3 = 12.4$
DeFu/2 images	$(FE + Cl) * 2 + DeFu (2 images)$	$(5.9 + 1.3) * 2 + 0.2 = 14.6$
DaFu/3 images	DaFu (3 images) + FE + Cl	$11.0 + 5.9 + 1.3 = 18.2$
DeFu/3 images	$(FE + Cl) * 3 + DeFu (3 images)$	$(5.9 + 1.3) * 3 + 0.2 = 21.8$
DaFu/4 images	DaFu (4 images) + FE + Cl	$16.6 + 5.9 + 1.3 = 23.8$
DeFu/4 images	$(FE + Cl) * 4 + DeFu (4 images)$	$(5.9 + 1.3) * 4 + 0.3 = 29.1$
DaFu/5 images	DaFu (5 images) + FE + Cl	$21.6 + 5.9 + 1.3 = 28.8$
DeFu/5 images	$(FE + Cl) * 5 + DeFu (5 images)$	$(5.9 + 1.3) * 5 + 0.3 = 36.3$
DaFu/6 images	DaFu (6 images) + FE + Cl	$27.7 + 5.9 + 1.3 = 34.9$
DeFu/6 images	$(FE + Cl) * 6 + DeFu (6 images)$	$(5.9 + 1.3) * 6 + 0.3 = 43.5$

and DeFu represents decision fusion. By observing Table 6, we find the average PCCs of decision fusion strategy are higher than those of data fusion strategy in most cases, except the average PCCs obtained when small intervals are used and less number of images are fused, which are labeled in bold in Table 6.

Table 7 shows the running times for recognizing unknown targets of the two fusion strategies under different number of images after preprocessing. As the training processes of the two strategies are identical, and the preprocessing procedures of the two strategies are also the same, we could only consider the running times for recognition of the two strategies after preprocessing. Computational Procedure recorded in Table 7 describes the calculation process of the running times of the two strategies under different number of images after preprocessing, where DaFu means the running time of the step of data fusion, FE means the running time of the step of feature extraction, Cl means the running time of the step of classification, and DeFu represents the running time of the step of decision fusion. The results of running times calculated are listed in the column of Time. From Table 7, we find the running time increases when the number of images used is growing both in the two strategies. Although the running times of the two strategies after preprocessing are relatively close, the operating efficiency of the data fusion strategy is slightly superior to the decision fusion strategy.

By observing Tables 6 and 7 and taking recognition rate and running time into account, we find that, if we only have two or three multi-aspect images of a target, and the aspect separations between the images are small (generally less than 20 degree), data fusion strategy

is the optimal choice for target recognition; if the aspect separations between the images are large (within the thresholds in Table 4), decision fusion strategy is the best choice for target recognition; if more than three multi-aspect images are acquired, and the aspect separations between images are within the thresholds in Table 4, decision fusion strategy is suggested to select for target recognition. Therefore, each of the fusion strategy appears to be better in different situations: data fusion for low number of images and small target aspect separations, and decision fusion for high number of images or large target aspect separations.

In conclusion, from the experimental results shown in this section, we know that if we have small number of multi-aspect images (six images are enough) and the aspect separations between those images are adequate, the recognition rate obtained by the proposed approaches can be advanced significantly compared with those obtained by single image. The reason for that is the amount of information obtained from multi-aspect images using fusion strategies is much more than that from single image. More information allows the improvement of recognition accuracy.

6. CONCLUSIONS AND DISCUSSING

We have investigated two different SAR image target recognition strategies using multi-aspect images of a target in this paper. Lots of experiments have been implemented to analyze the recognition performance of these two strategies. We have demonstrated that the performance of SAR image target recognition can be improved by using the proposed two strategies, if we took a small number of multi-aspect images of a target and the aspect separations between those images were proper, as the recognition performance was sensitive to the number of images and the aspect separations between them.

Our future research is to find other approaches using multi-aspect images of a target which may exploit the essence in multi-aspect images more efficiently and yield better outcomes. We may consider this issue mainly from two aspects. On one hand, super-resolution reconstruction approaches are to be studied for recognition performance improvement. As they can reconstruct a high-resolution image containing more details from multiple low-resolution SAR images belonged to the same target in different aspects. On the other hand, approaches not in a certain level but in multiple levels in SAR target recognition are taken into account for further advancing the recognition performance.

ACKNOWLEDGMENT

The work is supported by Zhejiang Provincial Natural Science Foundation of China (No. LQ12F04002) and the National Natural Science Foundation of China (No. 61204030). The work is also supported by Zhejiang Provincial Information Processing and Automation Technology Key Discipline Open Foundation of China.

REFERENCES

1. Mohammadpoor, M., R. S. A. Raja Abdullah, A. Ismail, and A. F. Abas, "A circular synthetic aperture radar for on-the-ground object detection," *Progress In Electromagnetics Research*, Vol. 122, 269–292, 2012.
2. Ross, T., S. Worrell, V. Velten, J. Mossing, and M. Bryant, "Standard SAR ATR evaluation experiments using the MSTAR public release data set," *Proc. SPIE*, Vol. 3370, 566–573, 1998.
3. Zhou, J., Z. Shi, X. Cheng, and Q. Fu, "Automatic target recognition of SAR images based on global scattering center model," *IEEE Trans. on Geoscience and Remote Sensing*, Vol. 49, No. 10, 3713–3729, 2011.
4. Sandirasegaram, N. and R. English, "Comparative analysis of feature extraction (2D FFT and wavelet) and classification (Lp metric distances, MLP NN, and HNeT) algorithms for SAR imagery," *Proc. SPIE*, Vol. 5808, 314–325, 2005.
5. Nilubol, C. and Q. H. Pham, "Translational and rotational invariant hidden Markov model for automatic target recognition," *Proc. SPIE*, Vol. 3374, 179–185, 1998.
6. O'Sullivan, J. A., M. D. DeVore, V. Kedia, and M. I. Miller, "SAR ATR performance using a conditionally Gaussian model," *IEEE Trans. on Aerospace and Electronic Systems*, Vol. 37, No. 1, 91–108, 2001.
7. Brown, M. Z., "Analysis of multiple-view Bayesian classification for SAR ATR," *Proc. SPIE*, Vol. 5095, 265–274, 2003.
8. Brendel, G. and L. Horowitz, "Benefits of aspect diversity for SAR ATR: Fundamental and experimental results," *Proc. SPIE*, Vol. 4053, 567–578, 2000.
9. Bhanu, B. and G. Jones, "Exploiting azimuthal variance of scatterers for multiple look SAR recognition," *Proc. SPIE*, Vol. 4727, 290–298, 2002.
10. Ettinger, G. and W. Snyder, "Model-based fusion of multi-look SAR for ATR," *Proc. SPIE*, Vol. 4727, 277–289, 2002.

11. Snyder, W. and G. Ettinger, "Performance models for hypothesis-level fusion of multi-look SAR ATR," *Proc. SPIE*, Vol. 5095, 396–407, 2003.
12. Vespe, M., C. Baker, and H. Griffiths, "Aspect dependent drivers for multi-perspective target classification," *IEEE Conference on Radar*, 256–260, 2006.
13. Anagnostopoulos, G. C., "SVM-based target recognition from synthetic aperture radar images using target region outline descriptors," *Nonlinear Analysis*, Vol. 71, e2934–e2939, 2009.
14. Wang, B., Y. Huang, J. Yang, and J. Wu, "A feature extraction method for synthetic aperture radar (SAR) automatic target recognition based on maximum interclass distance," *Sci. China Tech. Sci.*, Vol. 54, 2520–2524, 2011.
15. Liu, M., Y. Wu, P. Zhang, Q. Zhang, Y. Li, and M. Li, "SAR target configuration recognition using locality preserving property and Gaussian mixture distribution," *IEEE Trans. on Geoscience and Remote Sensing Letters*, Vol. 10, No. 2, 268–272, 2012.
16. Park, J., S. Park, and K. Kim, "New discrimination features for SAR automatic target recognition," *IEEE Geoscience and Remote Sensing Letters*, Vol. PP, No. 99, 1–5, 2012.
17. Chang, Y.-L., C.-Y. Chiang, and K.-S. Chen, "SAR image simulation with application to target recognition," *Progress In Electromagnetics Research*, Vol. 119, 35–57, 2011.
18. Zhao, Q., J. C. Principe, V. L. Brennan, D. Xu, and Z. Wang, "Synthetic aperture radar automatic target recognition with three strategies of learning and representation," *Opt. Eng.*, Vol. 39, No. 5, 1230–1244, 2000.
19. Zhao, Q. and J. C. Principe, "Support vector machines for SAR automatic target recognition," *IEEE Trans. on Aerospace and Electronic Systems*, Vol. 37, No. 2, 643–654, 2001.
20. Yang, W., Y. Liu, G.-S. Xia, and X. Xu, "Statistical mid-level features for building-up area extraction from high-resolution PolSAR imagery," *Progress In Electromagnetics Research*, Vol. 132, 233–254, 2012.
21. Vapnik, V. N., "An overview of statistical learning theory," *IEEE Trans. on Neural Networks*, Vol. 10, No. 5, 988–999, 1999.
22. Hsu, C. W. and C. J. Lin, "A comparison of methods for multiclass support vector machines," *IEEE Trans. on Neural Networks*, Vol. 13, No. 2, 415–425, 2002.
23. Huan, R. and Y. Pan, "Decision fusion strategies for SAR image target recognition," *IET Radar, Sonar and Navigation*, Vol. 5,

- No. 7, 747–755, 2011.
24. Huan, R. and R. Yang, “SAR automatic target recognition based on decision fusion,” *7th European Conference on Synthetic Aperture Radar (EUSAR)*, 1–4, 2008.
 25. Huan, R., K. Mao, Y. Lei, J. Yu, and M. Xia, “SAR target recognition with data fusion,” *2010 WASE International Conference on Information Engineering*, Vol. 2, 19–23, 2010.
 26. Rizvi, S. A. and N. M. Nasrabadi, “Fusion of automatic target recognition algorithms,” *Proc. SPIE*, Vol. 4726, 122–132, 2002.
 27. Rizvi, S. A. and N. M. Nasrabadi, “Fusion techniques for automatic target recognition,” *Proc. IEEE Conf. Applied Imagery Pattern Recognition Workshop*, 27–32, Washington DC, USA, 2003.